Polar amplification of Pliocene climate by elevated trace gas radiative forcing

Peter Hopcroft, Gilles Ramstein, Thomas Pugh, Stephen Hunter, Fabiola Murguia-Flores, Aurélien Quiquet, Yong Sun, Ning Tan, Paul Valdes

Polar amplification of Pliocene climate by elevated trace gas radiative forcing

Peter O. Hopcroft[a,1], Gilles Ramstein[b], Thomas A. M. Pugh[a,c], Stephen J. Hunter[d], Fabiola Murguia-Flores[e,f], Aurélien Quiquet[b,g], Yong Sun[b,h], Ning Tan[b,i], and Paul J. Valdes[e]

[a]School of Geography, Earth & Environmental Sciences, University of Birmingham, Birmingham B15 2TT United Kingdom; [b]Laboratoire des Sciences du Climat et de l'Environnement, Institut Pierre Simon Laplace, Commissariat à l'énergie atomique et aux énergies alternatives–Centre National de la Recherche Scientifique–Université de Saint-Quentin en Yvelines, Université Paris-Saclay, F-91191 Gif-sur-Yvette, France; [c]Birmingham Institute of Forest Research, University of Birmingham, Birmingham B15 2TT, United Kingdom; [d]School of Earth and Environment, University of Leeds, Leeds LS2 9JT, United Kingdom; [e]Bristol Research Initiative for the Dynamic Global Environment, School of Geographical Sciences, University of Bristol, Bristol BS8 1SS, United Kingdom; [f]Instituto de Investigaciones en Ecosistemas y Sustentabilidad, Universidad Nacional Autónoma de México, 58190 Morelia, Mexico; [g]Chair Energy and Prosperity, Institut Louis Bachelier, 75002 Paris, France; [h]State Key Laboratory of Numerical Modelling for Atmospheric Sciences and Geophysical Fluid Dynamics, Institute of Atmospheric Physics, Chinese Academy of Sciences, Beijing 100029, China; and [i]Key Laboratory of Cenozoic Geology and Environment, Institute of Geology and Geophysics, Chinese Academy of Sciences, Beijing 100029, China

Edited by John H. Seinfeld, California Institute of Technology, Pasadena, CA, and approved July 24, 2020 (received for review February 7, 2020)

Warm periods in Earth's history offer opportunities to understand the dynamics of the Earth system under conditions that are similar to those expected in the near future. The Middle Pliocene warm period (MPWP), from 3.3 to 3.0 My B.P, is the most recent time when atmospheric CO_2 levels were as high as today. However, climate model simulations of the Pliocene underestimate high-latitude warming that has been reconstructed from fossil pollen samples and other geological archives. One possible reason for this is that enhanced non-CO_2 trace gas radiative forcing during the Pliocene, including from methane (CH_4), has not been included in modeling. We use a suite of terrestrial biogeochemistry models forced with MPWP climate model simulations from four different climate models to produce a comprehensive reconstruction of the MPWP CH_4 cycle, including uncertainty. We simulate an atmospheric CH_4 mixing ratio of 1,000 to 1,200 ppbv, which in combination with estimates of radiative forcing from N_2O and O_3, contributes a non-CO_2 radiative forcing of 0.9 $W \cdot m^{-2}$ (range 0.6 to 1.1), which is 43% (range 36 to 56%) of the CO_2 radiative forcing used in MPWP climate simulations. This additional forcing would cause a global surface temperature increase of 0.6 to 1.0 °C, with amplified changes at high latitudes, improving agreement with geological evidence of Middle Pliocene climate. We conclude that natural trace gas feedbacks are critical for interpreting climate warmth during the Pliocene and potentially many other warm phases of the Cenezoic. These results also imply that using Pliocene CO_2 and temperature reconstructions alone may lead to overestimates of the fast or Charney climate sensitivity.

methane | Pliocene | GCM | trace gas | biogeochemistry | wetland

Introduction

The Middle Pliocene warm period around 3.3 to 3.0 My B.P. was the last period in Earth's history when atmospheric CO_2 was comparable to today's level, at approximately 400 ppmv (1–4). The Middle Pliocene warm period could therefore provide useful information on the response of the Earth system to greenhouse gas (GHG)-induced warming, that is relevant to the future evolution of the Earth system under continued anthropogenic GHG emissions (5–9). According to syntheses of reconstructed surface temperatures from geological archives on land (10) and in the ocean (11, 12), the Earth was globally warmer than the preindustrial, with a significant polar amplification especially in the Northern Hemisphere. The warmer conditions acted to reduce global ice volume, so that sea level was around 20 m higher than present (13–15).

The Pliocene Model Intercomparison Project (PlioMIP) is a coordinated study of climate model responses to Pliocene boundary conditions (16, 17) aimed at quantifying the underlying drivers of warmth during this time and to better understand the Earth System response to an atmospheric CO_2 concentration of ~400 ppmv. The results from the first phase (PlioMIP1) showed that coupled general circulation models (GCMs) failed to reproduce high-latitude warming seen in reconstructions (16). Several hypotheses could explain why the model simulations underestimate warming, including the role of orbitally induced climate variability (16), the configuration of ocean gateways and palaeogeography (e.g., refs. 18 and 19), and radiative forcing from trace gases other than CO_2 (20). While several studies have addressed the first three possibilities, the contributions of the atmospheric methane, nitrous oxide, and ozone (CH_4, N_2O, and O_3) have not been considered together.

At present, CH_4 is the second most important anthropogenic GHG after CO_2 (21). Its nearly threefold concentration increase since CE 1750 is responsible for approximately 25% of the GHG radiative forcing. We know that variations in CH_4 are huge in intensity and abrupt during the Anthropocene relative to the past several thousand years. Before widespread direct atmospheric monitoring, CH_4 could only be traced through air bubbles trapped in polar ice cores. These ice core records provide robust evidence that CH_4 is very sensitive to climate, with higher

Significance

Warm periods in Earth's history provide the only empirical evidence of how the climate system responds to raised atmospheric carbon dioxide (CO_2) levels. The Middle Pliocene, 3.3 to 3.0 My B.P., was the last time when CO_2 levels were as high as today. However, climate model simulations of the Pliocene underestimate the warming that has been reconstructed from geological archives. Using a numerical model of the global methane cycle we show that the inclusion of enhanced concentrations of non-CO_2 trace gases could have been responsible for an additional warming of 0.6 to 1.0 °C, with larger increases over northern land masses. These findings demonstrate the importance of trace gas climate forcing for both the Pliocene and potentially warm periods during much of Earth's recent history.

Author contributions: P.O.H., G.R., and P.J.V. designed research; P.O.H., T.A.M.P., S.J.H., F.M.-F., and N.T. performed research; A.Q., Y.S., and P.J.V. analyzed data; and P.O.H., G.R., T.A.M.P., A.Q., and P.J.V. wrote the paper.

The authors declare no competing interest.

This article is a PNAS Direct Submission.

[1]To whom correspondence may be addressed. Email: p.hopcroft@bham.ac.uk.

This article contains supporting information online at https://www.pnas.org/lookup/suppl/doi:10.1073/pnas.2002320117/-/DCSupplemental.

First published September 4, 2020.

values during warmer periods and with large-amplitude rapid variations during abrupt climate events (22, 23). Nitrous oxide (N_2O) also displays similar characteristics (24), while O_3 and many other important atmospheric constituents (e.g., OH) cannot be reconstructed from ice core gas samples. Before 800,000 y ago, variations in all trace gases with the exception of CO_2 are essentially unknown and must therefore be simulated using models (e.g., ref. 25).

Beerling et al. (26) simulated enhanced wetland emissions during the Pliocene but did not link this with other methane sources (26). Unger and Yue (20) (UY14 hereafter) simulated an increase in CH_4 lifetime by 23 to 31% during the Pliocene (for CH_4 = 1,000 to 2,000 ppbv) and an increase in tropospheric O_3 by 21 to 25% which contributed a radiative forcing of approximately 0.3 $W \cdot m^{-2}$. However, this CH_4 lifetime increase is partly caused by the self-feedback (e.g., ref. 27), a function of the prescribed CH_4 concentration in the model. Other than a model study of the Eocene and late Cretaceous superwarm periods (28), there is no comprehensive understanding of how trace gases may have affected pre-Quaternary warm periods like the Pliocene.

We address this with an ensemble of terrestrial biogeochemistry simulations for the Pliocene. In combination with climate fields from several GCM simulations of the Pliocene we develop an estimate of the Pliocene global CH_4 source, CH_4 sinks and thereby the CH_4 concentration, and CH_4 radiative forcing, including uncertainty. We combine these with estimates of N_2O and O_3 radiative forcing to evaluate how all of these trace gases may have determined the climate during the Pliocene.

Results

Emissions of CH_4 and Other Trace Gases. Our approach follows that used for modeling of the Quaternary CH_4 variations (25, 29, 30). We drive the Lund–Potsdam–Jena General Ecosystem Simulator (LPJ-GUESS) dynamic global vegetation model (31, 32) with climate simulations from four models used in the Pliocene Model Intercomparison Project phases 1 and 2 and simulate the key trace gas emissions at the land surface, including CH_4, emissions from wildfires, nonmethane biogenic volatile organic compounds (NMVOCs) from vegetation, and soil nitrogen oxides (NOx) (*SI Appendix*, Fig. S1). Assuming that the Pliocene is a quasi-equilibrium climate state, we do not account for any increased emissions from marine clathrates or permafrost which are likely more sensitive to abrupt warming (33). We use PlioMIP phase 1 (experiment 2) simulations (34) with Community Climate System Model 4 (CCSM4), Goddard Institute for Space Studies Model E2R (GISS-E2-R), and Institut Pierre-Simon Laplace Coupled Model 5A-LR (IPSL-CM5A-LR) and PlioMIP phase 2 (experiment with Pliocene orography and ice: Eoi^{400}) (16) simulations with IPSL-CM5A-LR and Hadley Centre Coupled Model 3 with Met Office Surface Exchange version 2.1 (HadCM3-M21). In all Pliocene climate model simulations the orography, land ice, and vegetation are based on geological reconstructions for the Pliocene (35, 36), and the mixing ratio of atmospheric CO_2 is increased from 280 ppbv in the preindustrial to 400 or 405 ppbv. We also incorporate HadCM3 PlioMIP phase 2 simulations performed with atmospheric CO_2 mixing ratios of 450 (37) and 490 ppmv which are labeled Eoi^{450} and Eoi^{490}, respectively. All climate simulations are described in *Materials and Methods*.

We estimate the CH_4 lifetime and the resultant concentration of CH_4 using a simplified offline one-box model of the atmospheric CH_4 chemistry (38) and radiative forcing (39). With this we do not resolve atmospheric transport or detailed chemical pathways, but we are able to quantify uncertainty by sampling the model stochastically. See *Materials and Methods* and *SI Appendix*, Table S2, for full details of all models used.

All CH_4 emissions increase in response to the simulated Pliocene climate conditions (*SI Appendix*, Table S1). Despite warmer and in many places wetter conditions (*SI Appendix*, Fig. S2), wetland area increases only marginally, but the emissions increase by 20 to 46%. Emissions increase notably in the Sahel region of North Africa in all models and in South Africa in all models except GISS. Elsewhere, emissions increase in Southeast Asia in all models except GISS and Australia in all models except CCSM4 and GISS. GISS shows the largest emissions increase of all models over the Amazon, whereas both IPSL simulations show a slight reduction in this region. A factor separation approach summarized in *SI Appendix*, Table S3, demonstrates that increased Pliocene temperature enhances emissions in all models. In HadCM3 and GISS, wetter soils also promote emissions but are less important in the other GCMs. Soil carbon stocks act to reduce emissions in HadCM3 and increase emissions in CCSM4 but have much less impact in the other models. Wildfire and termite emissions also increase by 50 to 83% and 21 to 37%, respectively and soil uptake (at pCH_4 = 715 ppmv) increases by 8 to 27%. Isoprene emissions increase by 5 to 40%, and monoterpene changes by −9 to +7%. These ranges span the different climate models used to drive each emissions scheme.

CH_4 Chemical Lifetime and Radiative Forcing. Although increased emissions will translate into elevated atmospheric concentration, the concentration is also dependent on the lifetime, which is influenced by other trace gas emissions and the physical state of the atmosphere. The change in CH_4 lifetime, Pliocene minus preindustrial, is summarized for each GCM in Fig. 1. Increased CH_4 emissions from wetlands, wildfires, and termites contribute a positive lifetime anomaly through the self-feedback effect. Additional NMVOC emissions (CO and isoprene) from wildfires and vegetation enhance the lifetime slightly. The higher global temperatures and associated humidity increase act to offset some of this lifetime increase in each model. This is because the reaction rate of CH_4 with OH scales with temperature, and the production of OH, which oxidizes CH_4, increases with water vapor availability and hence temperature (e.g., refs. 38 and 40). NMVOCs are the most model-dependent term, with a strong increase in emissions during the Pliocene in IPSL and HadCM3 but not in the other two GCMs. This is most likely a result of

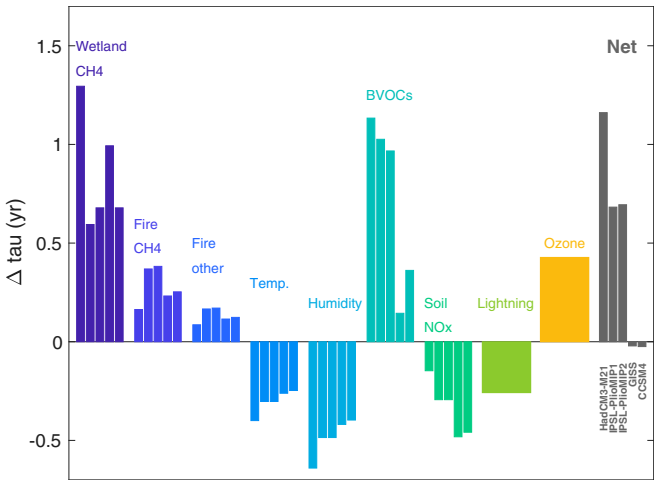

Fig. 1. Simulated mean change in lifetime of CH_4 with respect to OH for the Pliocene minus the preindustrial. Net values and individual terms are shown for the five different sets of climate drivers (HadCM3-M21-Eoi^{400}, IPSL-CM5A-PlioMIP1, IPSL-CM5A-Eoi^{400}, GISS-E2-R-PlioMIP1, and CCSM4-PlioMIP1).

the differences in the response of the tropical hydrological cycle. Soil NOx shows agreement across the four climate models. The results are also in agreement with the results of UY14. Lightning NOx increase and increased O_3 in the troposphere (both taken from UY14) have opposing influences on the Pliocene lifetime.

As the CH_4 lifetime is dependent on the CH_4 level, there is a nonlinearity which means that the total change in lifetime does not equal the sum of these individual terms. The net change is positive for HadCM3 and both IPSL simulations and very weakly negative in the other two models. This is mostly due to the much stronger BVOC emission term in the former two models.

The results of the sampling of the total Pliocene minus preindustrial CH_4 radiative forcing are shown in Fig. 2. The mean $\pm$ 1 SD anomalies are 0.16 ± 0.02, 0.20 ± 0.03, 0.21 ± 0.03, and 0.33 ± 0.05 $\mathrm{W \cdot m^{-2}}$ for CCSM4, GISS, IPSL, and HadCM3, respectively. The combined mean and 1σ range is 0.22 ± 0.07 $\mathrm{W \cdot m^{-2}}$. The total uncertainty in this estimate is dominated by the choice of climate simulation.

Discussion

Total Radiative Forcing. The global mean radiative forcing due to the CO_2 concentration of 400 ppm during the Pliocene is around 2.0 ± 0.3 $\mathrm{W \cdot m^{-2}}$. We approximate N_2O radiative forcing based on natural variations in these three GHGs through the late Quaternary as 15% of the combined CO_2 and CH_4 radiative forcing (41). Radiative forcing by O_3 is 0.29 $\mathrm{W \cdot m^{-2}}$ as simulated for CH_4 = 1,000 ppbv by UY14. This positive radiative forcing is partly due to a simulated increase in emissions of O_3 precursors, consistent with our simulated emissions (*SI Appendix*, Table S1). The uncertainty on the O_3 radiative forcing is calculated by scaling with the CH_4 concentration, which in three sensitivity simulations by ref. 20 shows an approximately logarithmic dependence. O_3 is also created as a by-product of CH_4 emissions; thus, it is partially included in the O_3 radiative forcing and in our indirect CH_4 radiative forcing. Hence, we reduce our total forcing using the combined factor for O_3 radiative forcing from CH_4 as in *SI Appendix*, Table S4, to avoid double counting. Together with a CH_4 radiative forcing, we derive an approximate radiative forcing due to other non-CO_2 well-mixed GHGs of 0.8 (0.72 to 1.02) $\mathrm{W \cdot m^{-2}}$ as summarized in Table 1.

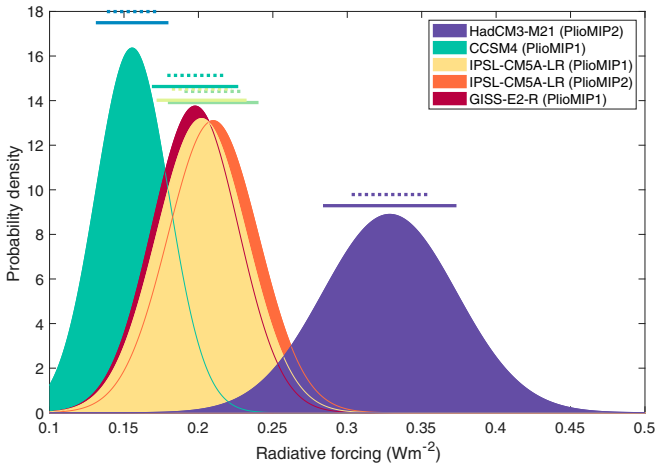

Fig. 2. Estimated radiative forcing expressed as a probability density function. The uncertainty stems from 1) assumed $\pm$20% uncertainties in lightning NOx and tropospheric O_3, 2) uncertainty in the parameters used to estimate OH lifetime of CH_4 (38), and 3) uncertainty in the total radiative forcing due to CH_4 (38, 39). The ± 1 σ uncertainty is shown above each curve. Dashed lines represent the first two factors, and solid bars underneath include all three sources of uncertainty.

The rate of methane radiative forcing increase per degree of global mean temperature change (see also ref. 42) is a useful property to compare time periods or models. We denoted this as γ_{fCH4}, and it ranges from 89 to 113 $\times$ $10^{-3}\mathrm{Wm^{-2}K^{-1}}$ across the five climate model simulations, with the lowest value simulated by CCSM4 and the highest by HadCM3. This range slightly exceeds the observed value of 68 (57 to 85) $\times$ $10^{-3}\mathrm{Wm^{-2}K^{-1}}$ derived from the last glacial maximum to the late-Holocene preindustrial (22, 43). It is consistent with simulated values of 97 to 119 $\times$ $10^{-3}\mathrm{Wm^{-2}K^{-1}}$ for the Early Eocene and 89 $\times$ $10^{-3}\mathrm{Wm^{-2}K^{-1}}$ for the Late Cretaceous calculated with a coupled climate–chemistry modeling framework (28), for which the direct radiative forcing values have been augmented here following a recent update (39).

The Pliocene climate may have induced changes in the emissions and lifetime of natural aerosols. UY14 simulated a net cooling by nitrate, particulate organic matter, and biogenic secondary organic aerosols (SOA) and a warming effect from black carbon, leading to a negative aerosol forcing of -0.4 $\mathrm{W \cdot m^{-2}}$ (20). We simulate smaller changes in emissions from biomass burning (+50 to 84% versus +101% by UY14) and BVOCs (precursors of SOA, +5 to 40% versus +50% by UY14), and so this would likely equate to a smaller net forcing. Other aerosol changes may have a warming effect. For example, mineral dust levels are generally lower in warm climates, and deserts contracted during the Pliocene (10). Interactions of CH_4 with nitrate and sulfate can also enhance radiative forcing (44). Pliocene aerosol effects therefore require further study.

The climate simulations could be benchmarked with Pliocene climate reconstructions. Though no global compilations of precipitation change are available for the Pliocene, individual records can provide informative constraints. The West African monsoon was probably stronger during the Middle Pliocene even when compared to the early to middle Holocene (45). There was also a general drying trend in East Africa during the Pliocene (46), which, if continued to the present, implies wetter conditions during the Middle Pliocene. Both of these features are most faithfully reproduced in HadCM3 and GISS and the Eoi^{400} IPSL simulation (*SI Appendix*, Fig. S2). In Asia, a reconstructed near-doubling of precipitation in southern China (47) is replicated in IPSL (Eoi^{400} simulation) and by HadCM3 but not the other models. Only HadCM3 and CCSM4 simulate wetter conditions reconstructed for the early to middle Pliocene in Australia (48). One of the regions of largest intermodel spread in precipitation is tropical South America, but to our knowledge, quantitative precipitation records have yet to be produced.

HadCM3 has the strongest warming globally and in particular over most land masses and over the North Atlantic, where most other models significantly underestimate reconstructed warming (6). HadCM3 model also shows among the best agreement with the available temperature reconstructions (10). This lends support to the stronger methane forcing that is simulated with the HadCM3 climate drivers since the enhanced warming, particularly over land and associated hydrological cycle changes, promote trace gas emissions. A global biome reconstruction could also provide some measure to discern between simulations (49), but this is initially derived from a simulation with HadCM3 and so is very likely biased toward the climatic response of this model.

Likely Non-CO_2 Climatic Response. Our modeling study probably underestimates the true magnitude of the Pliocene methane cycle feedback because the climate and methane cycle are not coupled. The feedback of methane radiative forcing via climate to methane emissions is not complete, and all of the simulated climates underestimate midlatitude and high-latitude warming over land considerably (10). Furthermore, our study has a relatively modest change in wetland area compared with modeling

Table 1. Pliocene radiative forcing, CH_4 cycle sensitivity, and predicted non-CO_2-forced warming from this study and past work

	Mean	Range	Reference
Radiative forcing ($W{\cdot}m^{-2}$)			
CO_2	2.0	–	Haywood et al. (17)
CH_4	0.22	0.10–0.43	This study
N_2O	0.33	0.32–0.36	This study
O_3	0.29	0.28–0.36	Unger and Yue (20)
Total GHG	2.80	2.67–3.02	This study
Total non-CO_2	0.80	0.67–1.02	This study
With self-feedback	0.86	0.72–1.12	This study
% of CO_2	43%	36–56%	This study
CH_4 cycle sensitivity to Temperature ($\times 10^{-3} Wm^{-2}K^{-1}$)			
Pliocene (3.3–3.0 Ma BP)	100	89–114	This study
Early Eocene (55 Ma BP)	109	97–120	Beerling et al. (28)
Cretaceous (90 Ma BP)	89	–	Beerling et al. (28)
LGM (21 ka BP)	68	57–85	Loulergue et al. (22) and Annan and Hargreaves (43)
Global mean temperature change (°C)			
Warming (non-CO_2)	0.7	0.6–0.9	This study
With self-feedback	0.7	0.6–1.0	This study

studies of earlier warm periods (26, 28, 50), and so the resultant radiative forcing is potentially a conservative prediction. Any additional warming resulting from the higher concentrations of trace gases including methane would further perturb the sources and atmospheric chemistry. Using the upper and lower limits for the γ_{fCH4}, we can approximate this. The trace gas forcing-induced warming would lead to an additional methane feedback bringing the total Pliocene methane radiative forcing to 0.72 to 1.1 $W{\cdot}m^{-2}$. These total non-CO_2 values are 36 to 56% of the CO_2 radiative forcing, with a central estimate of 0.9 $W{\cdot}m^{-2}$ or 43% of the CO_2 forcing. This would cause a warming of 0.6 to 1.0 °C (Table 1).

This is an important additional warming signal given that PlioMIP phase 1 GCMs forced only with increased CO_2 show a response of 2.7 ± 0.8 K (16). To better understand the regional impacts of this additional radiative forcing we analyze Middle Pliocene simulations from HadCM3 with prescribed levels of atmospheric CO_2. The CO_2 radiative forcing differences relative to the default Eoi^{400} are approximately 0.66 $W{\cdot}m^{-2}$ for the increase by 50 ppmv and 1.1 $W{\cdot}m^{-2}$ for the increase to 490 ppmv. These encompass the range of non-CO_2 GHG radiative forcing we calculated (0.72 to 1.1 Wm^2). The effective radiative forcing (or the temperature change per unit increment of radiative forcing) is actually higher for CH_4 and N_2O than for CO_2, and it is lower for O_3 (51). For simplicity here we assume that they are all equal.

The Pliocene HadCM3 simulations with differing CO_2 concentrations show significant polar amplification, especially in the Northern Hemisphere and around the Atlantic (Fig. 3). The Eoi^{450} and Eoi^{490} simulations show relatively muted warming signal in the circum-Atlantic because of a reduction in heat transport in the Atlantic (37). The upper end of our estimated radiative forcing, represented by the Eoi^{490} simulation, is shown in Fig. 3*B*. This estimated non-CO_2 GHG radiative forcing (Fig. 3*C*) causes high-latitude temperatures to increase by around 1 to 2.5 °C over land and by 1 to 2 °C over the ocean surface (Fig. 3 and *SI Appendix*, Fig. S3). This does not eliminate the large mismatches found over high-latitude Asia (Fig. 3 *C* and *D*) and in the North Atlantic (*SI Appendix*, Fig. S3), but it improves the comparison with the temperature reconstructions by ref. 10 as shown in Fig. 3*D*. The distribution of errors is shifted from having a significant probability over the range −5 to −1 °C to being approximately centered on 0 °C. For HadCM3, both the smaller and larger increases in radiative forcing improve the model–data agreement, except for sites with very high temperatures at high latitudes. The very high temperatures in high-latitude regions would very likely further enhance trace gas emissions, especially CH_4 from wetlands, and so reinforce the positive radiative forcing.

Reasons for the enduring high-latitude discrepancies might include seasonal bias in reconstructions over land or ocean (52) and long-term trends in seawater chemistry (53). If the reconstructions capture peak warmth during orbital cycles, this may not be adequately captured by climate model simulations with preindustrial orbital configuration (54), and global assemblages of reconstructions may capture different phases of Earth's orbit in different locations (10), further complicating comparisons with simulations. Terrestrial reconstructions are also potentially influenced by the dependence of plant water use efficiency on atmospheric CO_2 and changes in seasonality and the frequency of extreme events (55). However, a general underestimation in polar amplification of past warm states could signify systematic problems with climate model parameterizations of clouds (56, 57) and/or aerosol–cloud interactions (58).

These model results allow an estimate of $S_{LI,GHG}$, the temperature response per unit of radiative forcing due to ice sheets and sea level (LI) and due to GHGs ($K/W{\cdot}m^{-2}$), where S_{LI,CO_2} was possible until now (4). Several studies have considered the Earth system sensitivity, the long-term temperature response to changes in radiative forcing, incorporating vegetation and ice sheet responses (5). Our central estimate of 43% non-CO_2 GHG radiative forcing would reduce values estimated from Pliocene temperature reconstructions from around 9 °C (59) to 6.5 °C. This is still much larger than predicted based on fast feedbacks in the climate system and is therefore potentially consistent with irreversible long-term planetary warming, should we fail to limit warming this century to 1.5 °C (8).

Conclusions

The Middle Pliocene is a critically important past time period to understand because levels of atmospheric CO_2 were very likely as high as today's anthropogenically perturbed levels, at around 400 ppmv. The Pliocene therefore offers unique insight into a warmer Earth system at equilibrium (5, 6). CH_4 is the second most important anthropogenic GHG today, but beyond the ice core era to 800 ka BP, it has been largely ignored. Whereas

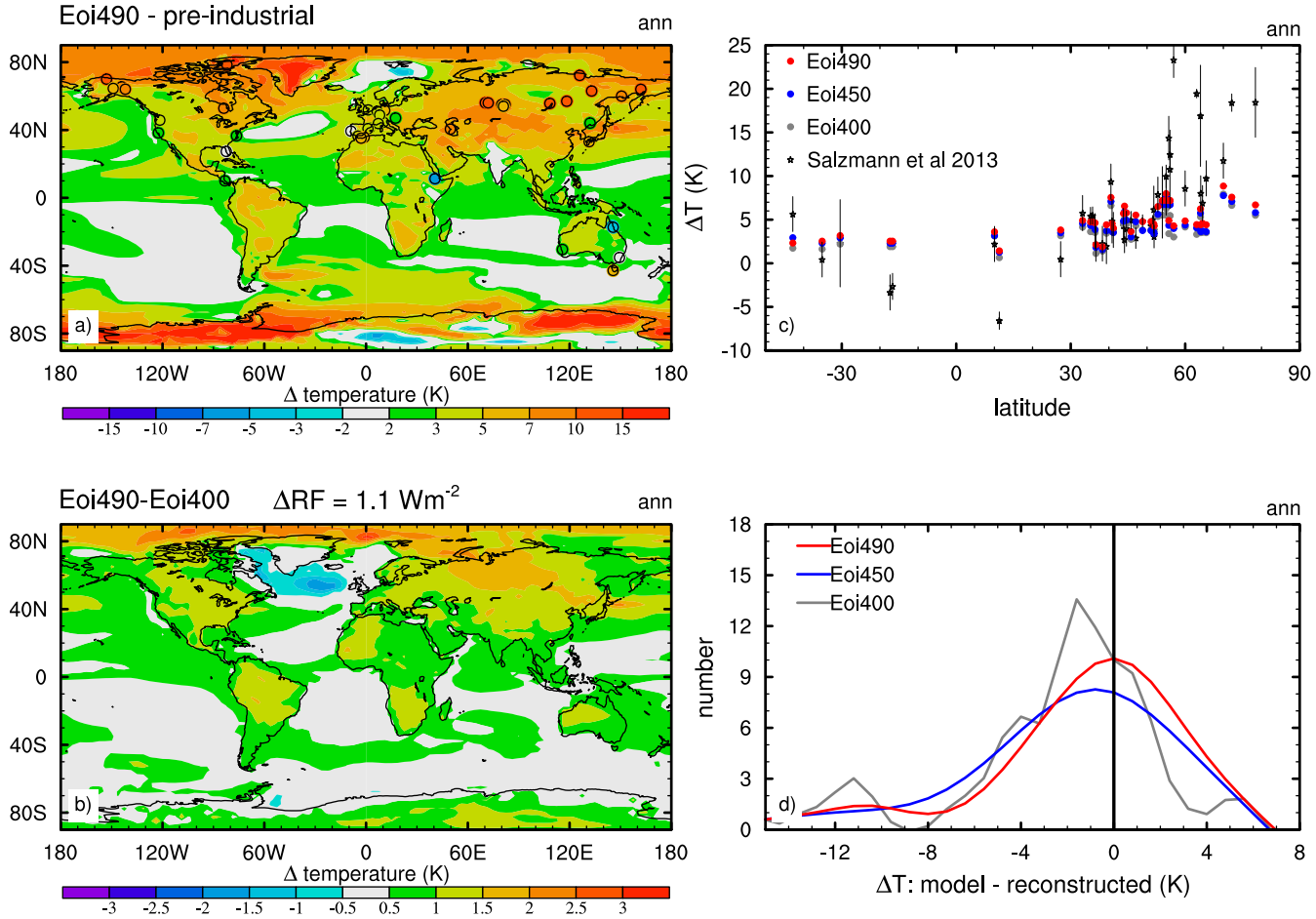

Fig. 3. Simulations with HadCM3-M21 and reconstructions of Pliocene near-surface air temperature change (ΔT) relative to the preindustrial (K). (*A*) Simulated (37) and reconstructed (10) ΔT for Eoi^{490} minus preindustrial, (*B*) simulated ΔT for Eoi^{490} − Eoi^{400}, (*C*) latitudinal comparison of the reconstructed and simulated temperature anomalies, and (*D*) histogram of model minus reconstruction temperature anomalies.

for CO_2, proxies have been developed to reconstruct its evolution for deep times, no such proxy exists for CH_4. We used vegetation model simulations and an offline CH_4 budget model to produce a comprehensive set of simulations quantifying the likely CH_4 emissions, lifetime, and concentration during this time period, investigating changes of methane sources and sinks but excluding abrupt releases derived from clathrates or permafrost degradation. We show that there is a direct net positive radiative forcing of 0.22 $W \cdot m^{-2}$ (range 0.1 to 0.45), which when combined with estimates of radiative forcing from N_2O and O_3 leads to an additional radiative forcing that is between 36 and 56% of that caused by a CO_2 concentration of 400 pmv. This would likely cause an additional global mean warming of approximately 0.6 to 1.0 °C at the global scale. Terrestrial trace gas radiative forcing is therefore critically important for understanding the reconstructed warmth of the Pliocene. We suggest that the first-order estimates of these additional forcing agents could help to reconcile model and proxy-based estimates of Pliocene warmth and that failing to include such forcings will lead to substantial biases in simulations of past climates. Their omission also has consequences when trying to estimate the fast or Charney climate sensitivity from paleodata (60). Such methods attempt to remove the slower Earth system forcings such as changes in ice sheets and assume the residual changes are due to the fast response to CO_2. However, these estimates have not normally included non-CO_2 trace gases and are therefore potentially overestimating the CO_2 sensitivity.

Materials and Methods

Climate Simulations. We use climate simulations from four GCMs: HadCM3-M21, IPSL-CM5A-LR, CCSM4, and GISS-E2-R. These GCMs are compared briefly in *SI Appendix*, Table S2. They span a reasonable range of changes for Pliocene and incorporate either PlioMIP phase 1 experiment 2 (34, 61) or PlioMIP phase 2 boundary conditions for the Pliocene (17). In all Pliocene simulations, the CO_2 mixing ratio is increased from 280 ppmv in the preindustrial to 400 (PlioMIP2) or 405 ppmv (PlioMIP1). The remaining Pliocene boundary conditions are based on geological evidence for orography, land ice, vegetation, and soils or are left unchanged at preindustrial settings. For land ice, the volume of the Greenland ice sheet is reduced, and the West Antarctic ice sheet is removed. Eustatic sea level is 25 m above modern. The global vegetation reconstruction prescribes a northward extension of forests causing a reduction in the area of tundra, while deserts are partly replaced by savannah and forest, particularly in the Sahel (10). In PlioMIP phase 1 simulations, orography increases over the Rockies and East Antarctica, but these changes are smaller in PlioMIP phase 2 for which both the Canadian Archipelago and Bering Strait are closed. The remaining model boundary conditions, including orbital configuration, solar constant, mixing ratios of CH_4, N_2O, and O_3, and aerosols are as used in the relevant preindustrial setup.

In PlioMIP1 phase 1, the boundary conditions are referred to as experiment 2 for coupled atmosphere–ocean simulations (34, 61). In PlioMIP phase 2 the nomenclature used is Ex^c, where x can include o and/or i to signify whether or not the orography and land ice, respectively, are based on Pliocene geological reconstructions, and c is the prescribed Pliocene CO_2 mixing ratio (17). Since the default PlioMIP phase 2 CO_2 mixing ratio is 400 ppmv, this simulation is labeled Eoi^{400}. We also make use of simulations with HadCM3-M21 in which the CO_2 mixing ratio is set to 450 or 490 ppmv, and these are labeled Eoi^{450} and Eoi^{490}, respectively. The global mean

radiative forcing difference relative to the standard Eoi^{400} simulation is therefore approximately 0.7 and 1.1 $W{\cdot}m^{-2}$, for Eoi^{450} and Eoi^{490}, respectively. These increases therefore encompass the upper and lower ends of our estimated additional non-CO_2 radiative forcing listed in Table 1.

Vegetation Model Simulations. We simulate the land surface with the dynamic stand-based global vegetation model LPJ-GUESS v3 (31, 32). LPJ-GUESS was forced with repeating 30 y of monthly fields from the four GCMs listed above. A 500-y spin up to equilibrium was conducting using repeating the 30-y climate data prior to each 30-y simulation. We expand the land–sea mask using coastlines from PlioMIP phase 2 (17), including a partially deglaciated Greenland. The soil type over new land points is extrapolated from nearby existing points using the default soil type in LPJ-GUESS. CO_2 was set to 280 and 400 ppmv for preindustrial and Pliocene simulations, respectively.

Trace Gas Emissions. Wetland area is calculated from the GCM soil moisture using a TOPMODEL (TOPography based hydrological MODEL) approach (62), in which the fractional area of inundation is calculated from the probability density function within each grid cell as derived from global high-resolution topographic data. CH_4 emissions are a function of microbial activity, i.e., temperature, available substrate, and wetland area (63). Total preindustrial emissions are scaled to 140 $TgCH_4/y$ for each model, consistent with the observed methane isotope and concentration measurements (64).

Termite CH_4 emissions are calculated from the LPJ-GUESS simulated plant functional types coverage and observed emission per biome type (30, 65). Isoprene and monoterpene emissions and biomass burning are represented with process-based schemes coupled within LPJ-GUESS (66–68). We estimate soil emissions of nitrogen oxides (NOx) using a recently developed semiempirical scheme (69).

CH_4 Chemical Lifetime and Radiative Forcing. We calculate the uptake of CH_4 in soils with a process-based model (70) driven with climatologies from the GCMs. For the OH lifetime τ, we integrate the Pliocene changes in emissions of all of the above species as well as atmospheric conditions and composition. As a full three-dimensional chemistry-transport simulation is extremely computationally expensive, it would limit the evaluation of uncertainty. Hence, we employ a parametric model (38) which is calibrated with three coupled climate–chemistry transport models. This model is described in *SI Appendix*.

We combine the CH_4 source estimates with the lifetime calculation in a global mean budget calculation $B = S \times \tau$, where B is the atmospheric CH_4 burden in Tg, S is the global mean CH_4 source, and τ is the lifetime in years (64). The budget equation is combined with the parametric lifetime model and the soil uptake, which is multiplied by the resultant concentration divided by preindustrial value. This is solved iteratively, to account for the self-feedback of CH_4 on lifetime and soil uptake.

The methane radiative forcing is a combination of direct and indirect components which are given in *SI Appendix*, Table S4. The total is 0.8 ± 0.09 $W{\cdot}m^{-2}$ per 1,000 ppbv increase in atmospheric CH_4.

To account for uncertainties, we prescribe a standard deviation of $\pm 20\%$ for lightning NOx and stratospheric O_3, which are not simulated directly. We include uncertainties inherent in the CH_4 lifetime and radiative forcing calculations as described in *SI Appendix*, and an example is shown in *SI Appendix*, Table S5. The calculations are sampled with 10,000 evaluations of the iterated global CH_4 budget formulation.

Data Availability. GCM simulation output for the preindustrial simulations are available from Earth System Grid Federation Coupled Model Intercomparison Project Phase 5 archive. Pliocene simulations can be obtained through the PlioMIP project. Pliocene geographic boundary conditions used in this study are available from Pliocene Research, Interpretation, and Synoptic Mapping: https://geology.er.usgs.gov/egpsc/prism/4_data.html. LPJ-GUESS model outputs and all model code developed in this study have been archived on figshare: https://doi.org/10.6084/m9.figshare.12302201 (piControl simulations), https://doi.org/10.6084/m9.figshare.12302216 (PlioMIP1 simulations), https://doi.org/10.6084/m9.figshare.12302228 (PlioMIP2 simulations), and https://doi.org/10.6084/m9.figshare.12344027 (emissions and lifetime code). The source code for LPJ-GUESS v4.0 can be obtained on request through Lund University (http://web.nateko.lu.se/lpj-guess). HadCM3-M21 Eoi^{490} climate fields are archived on figshare: https://doi.org/10.6084/m9.figshare.12630356.

ACKNOWLEDGMENTS. P.O.H. is supported by a University of Birmingham Fellowship. G.R. is supported by the French project Les Enveloppes Fluides et l'Environnement "ComPreNdrE" (A2016-992936), French State Program Investissements d'Avenir (managed by Agence Nationale de la Recherche [ANR]), ANR Human Ancestors Dispersal: the role of Climate project, Grant ANR-17-CE31-0010 of the French National Research Agency. T.A.M.P. acknowledges support from the European Research Council under the European Union Horizon 2020 program (Grant 758873, TreeMort). This work was carried out using the computational facilities of the Birmingham Environment for Academic Research (http://www.bear.bham.ac.uk). We thank Linda Sohl and Mark Chandler from NASA GISS for providing model outputs and Nan Rosenbloom (National Center for Atmospheric Research) who performed the original CCSM4 simulations. We thank Sophie Szopa for informative discussions on these topics. This is paper number 48 of the Birmingham Institute of Forest Research.

1. O. Seki *et al.*, Alkenone and boron-based Pliocene pCO2 records. *Earth Planet Sci. Lett.* **292**, 201–211 (2010).
2. G. Bartoli, B. Honisch, R. Zeebe, Atmospheric CO2 decline during the Pliocene intensification of Northern Hemisphere glaciations. *Paleoceanography* **26**, PA4213 (2011).
3. M. Badger, D. Schmidt, A. Mackensen, R. Pancost, High resolution alkenone palaeobarometry indicates relatively stable pCO2 during the Pliocene (3.3 to 2.8 Ma). *Philos. Trans. R. Soc. A* **371**, 20130094 (2013).
4. M. A. Martinez-Boti *et al.*, Plio-Pleistocene climate sensitivity evaluated using high-resolution CO2 records. *Nature* **518**, 49–54 (2015).
5. D. J. Lunt *et al.*, Earth system sensitivity inferred from Pliocene modelling and data. *Nat. Geosci.* **3**, 60–64 (2010).
6. A. M. Haywood, H. J. Dowsett, A. M. Dolan, Integrating geological archives and climate models for the mid-Pliocene warm period. *Nat Commun* **7**, 10646 (2016).
7. K. D. Burke *et al.*, Pliocene and Eocene provide best analogs for near-future climates. *Proc. Natl. Acad. Sci. U. S. A.* **115**, 13288–13293 (2018).
8. W. Steffen *et al.*, Trajectories of the Earth system in the Anthropocene. *Proc. Natl. Acad. Sci. U. S. A.* **115**, 8252–8259 (2018).
9. N. Tan *et al.*, Modeling Greenland ice sheet evolution during the Plio-Pleistocene transition: New constraints for pCO2 pathway. *Nat. Commun.* **9**, 4755 (2018).
10. U. Salzmann *et al.*, Challenges in quantifying Pliocene terrestrial warming revealed by data-model discord. *Nat. Clim. Change* **3**, 969–974 (2013)
11. H. J. Dowsett *et al.*, Sea surface temperature of the mid-Piacenzian ocean: A data-model comparison. *Sci. Rep.* **3**, 2013 (2013)
12. K. Foley, H. Dowsett, Data from "Community sourced mid-Piacenzian sea surface temperature (SST) data." US Geological Survey. http://doi.org/10.5066/P9YP3DTV. Accessed 24 September 2019.
13. K. G. Miller *et al.*, High tide of the warm Pliocene: Implications of global sea level for Antarctic deglaciation. *Geology* **40**, 407–410 (2012).
14. A. Dutton *et al.*, Sea-level rise due to polar ice-sheet mass loss during past warm periods. *Science* **349**, aaa4019 (2015)
15. O. A. Dumitru *et al.*, Constraints on global mean sea level during Pliocene warmth. *Nature* **574**, 233–236 (2019).
16. A. M. Haywood *et al.*, Large-scale features of Pliocene climate: Results from the Pliocene Model Intercomparison Project. *Clim. Past* **9**, 191–209 (2013).
17. A. M. Haywood *et al.*, The Pliocene Model Intercomparison Project (PlioMIP) Phase 2: Scientific objectives and experimental design. *Clim. Past* **12**, 663–675 (2016).
18. M. M. Robinson *et al.*, Bathymetric controls on Pliocene North Atlantic and Arctic sea surface temperature and deepwater production. *Palaeogeogr. Palaeoclimatol. Palaeoecol.* **309**, 92–97 (2011).
19. B. L. Otto-Bliesner *et al.*, Amplified North Atlantic warming in the late Pliocene by change in Arctic gateways. *Geophys. Res. Lett.*, **44**, 957–964 (2017).
20. N. Unger, X. Yue, Strong chemistry-climate feedbacks in the Pliocene. *Geophys. Res. Lett.* **41**, 527–533 (2014).
21. G. Myhre *et al.*, "Anthropogenic and natural radiative forcing" in *Climate Change 2013: The Physical Science Basis: Contribution of Working Group I to the Fifth Assessment Report of the Intergovernmental Panel on Climate Change*, T. Stocker *et al.*, Eds. (Cambridge University Press, Cambridge, United Kingdom, 2013), pp. 659–740.
22. L. Loulergue *et al.*, Orbital and millennial-scale features of atmospheric CH_4 over the past 800,000 years. *Nature* **453**, 383–386 (2008).
23. R. Rhodes *et al.*, Enhanced tropical methane production in response to iceberg discharge in the North Atlantic. *Science* **348**, 1016–1019 (2015).
24. A. Schilt *et al.*, Glacial-interglacial and millennial scale variations in the atmospheric nitrous oxide concentration during the last 800,000 years. *Quat. Sci. Rev.* **29**, 182–192 (2010).
25. P. J. Valdes, D. J. Beerling, C. E. Johnson, The ice age methane budget. *Geophys. Res. Lett.* **32**, L02704 (2005).
26. D. Beerling, R. A. Berner., F. T. Mackenzie, M. B. Harfoot, J. A. Pyle, Methane and the CH_4-related greenhouse effect over the past 400 million years. *Am. J. Sci.* **309**, 97–113 (2009).
27. C. D. Holmes Methane feedback on atmospheric chemistry: Methods, models, and mechanisms. *J. Adv. Model. Earth Syst.* **10**, 1087–1099 (2018).
28. D. J. Beerling, A. Fox, D. S. Stevenson, P. J. Valdes, Enhanced chemistry-climate feedbacks in past greenhouse worlds. *Proc. Natl. Acad. Sci. U.S.A.* **108**, 9880–9775 (2011).

29. J. S. Singarayer, P. J. Valdes, P. Friedlingstein, S. Nelson, D. J. Beerling, Late Holocene methane rise caused by orbitally controlled increase in tropical sources. *Nature* **470**, 82–85 (2011).
30. P. O. Hopcroft, P. J Valdes, F. M. O'Connor, J. O. Kaplan, D. J. Beerling, Understanding the glacial methane cycle. *Nat. Commun.* **8**, 14383 (2017).
31. B. Smith, I. C. Prentice, M. T. Sykes, Representation of vegetation dynamics in the modelling of terrestrial ecosystems: Comparing two contrasting approaches within European climate space. *Global Ecol. Biogeogr.* **10**, 621–637 (2001).
32. B. Smith *et al.*, Implications of incorporating N cycling and N limitations on primary production in an individual-based dynamic vegetation model. *Biogeosciences* **11**, 2027–2054 (2014).
33. C. D. Ruppel, J. D. Kessler, The interaction of climate change and methane hydrates. *Rev. Geophys.* **55**, 126–168 (2017).
34. A. M. Haywood *et al.*, Pliocene Model Intercomparison Project (PlioMIP): Experimental design and boundary conditions (experiment 2). *Geosci. Model Dev.* **4**, 571–577 (2011).
35. H. Dowsett *et al.*, The PRISM3D paleoenvironmental reconstruction. *Stratigraphy* **7**, 123–139 (2010).
36. H. Dowsett *et al.*, The PRISM4 (mid-Piacenzian) paleoenvironmental reconstruction. *Clim. Past* **12**, 1519–1538 (2016).
37. S. J. Hunter, A. M. Haywood, A. M. Dolan, J. C. Tindall, The HadCM3 contribution to PlioMIP phase 2. *Clim. Past* **15**, 1691–1713 (2019).
38. C. D. Holmes, M. J. Prather, O. A. Sovde, G. Myhre, Future methane, hydroxyl, and their uncertainties: Key climate and emission parameters for future predictions. *Atmos. Chem. Phys.* **13**, 285–302 (2013).
39. M. Etminan, G. Myhre, E. J. Highwood, K. P. Shine, Radiative forcing of carbon dioxide, methane, and nitrous oxide: A significant revision of the methane radiative forcing. *Geophys. Res. Lett.* **43**, 12614–12623 (2017).
40. A. Voulgarakis *et al.*, Analysis of present day and future OH and methane lifetime in the ACCMIP simulations. *Atmos. Chem. Phys.* **13**, 2563–2587 (2013).
41. J. Hansen *et al.*, Climate change and trace gases. *Philos. Trans. R. Soc. A* **365**, 1925–1954 (2007).
42. B. Ringeval *et al.*, Climate-CH_4 feedback from wetlands and its interaction with the climate-CO_2 feedback. *Biogeosciences* **8**, 2137–2157 (2011).
43. J. D. Annan, J. C. Hargreaves, A new global reconstruction of temperature changes at the Last Glacial Maximum. *Clim. Past* **9**, 367–376 (2013).
44. D. T. Shindell *et al.*, Improved attribution of climate forcing to emissions. *Science* **326**, 716–718 (2009).
45. R. R. Kuechler, L. M. Dupont, E. Schefuss, Hybrid insolation forcing of Pliocene monsoon dynamics in West Africa. *Clim. Past* **14**, 73–84 (2018).
46. H. M. Liddy, S. J. Feakins, J. E. Tierney, Cooling and drying in northeast Africa across the Pliocene. *Earth Planet Sci. Lett.* **449**, 430–438 (2016).
47. T. Su *et al.*, Post-Pliocene establishment of the present monsoonal climate in SW China: Evidence from the late Pliocene Longmen megaflora. *Clim. Past* **9**, 1911–19020 (2013).
48. B. Christensen *et al.*, Indonesian throughflow drove Australian climate from humid Pliocene to arid Pleistocene. *Geophys. Res. Lett.* **44**, 6914–6925 (2017).
49. U. Salzmann, A. M. Haywood, D. J. Lunt, P. J. Valdes, D. J. Hill, A new global biome reconstruction and data-model comparison for the Middle Pliocene. *Global Ecol. Biogeogr.* **17**, 432–447 (2008).
50. D. J. Wilton *et al.*, A predictive algorithm for wetlands in deep time paleoclimate models. *Geosci. Model Dev.* **12**, 1351–1364 (2019).
51. J. Hansen, Efficacy of climate forcings. *J. Geophys. Res.* **110**, D18104 (2005).
52. J. E. Tierney, M. P. Tingley, BAYSPLINE: A new calibration for the alkenone paleothermometer. *Palaeoceanogr. Paleoclimatol.* **33**, 281–301 (2016).
53. D. Evans *et al.*, Planktic foraminifera shell chemistry response to seawater chemistry: Pliocene–Pleistocene seawater Mg/Ca, temperature and sea level change. *Earth Planet Sci. Lett.* **438**, 139–148 (2016).
54. C. L. Prescott *et al.* Assessing orbitally-forced interglacial climate variability during the mid-Pliocene Warm Period. *Earth Planet Sci. Lett.* **400**, 261–271 (2014).
55. S. P. Harrison, P. J. Bartlein, I. C. Prentice, What have we learnt from palaeoclimate simulations?. *J. Quat. Sci.* **31**, 364–385 (2016).
56. N. Sagoo, P. Valdes, R. Flecker, L. J. Gregoire, The early Eocene equable climate problem: Can perturbations of climate model parameters identify possible solutions? *Philos. Trans. R. Soc. A* **371**, 20130123 (2013).
57. J. Zhu, C. J. Poulsen, J. E. Tierney, Simulation of Eocene extreme warmth and high climate sensitivity through cloud feedbacks. *Sci. Adv.* **5**, eaax1874 (2019).
58. J. T. Kiehl, C. A. Shields, Sensitivity of the Palaeocene-Eocene Thermal Maximum climate to cloud properties. *Philos. Trans. R. Soc. A* **371**, 20130093 (2013).
59. M. Pagani, Z. Liu, J. LaRiviere, A. C. Ravel, High Earth-system climate sensitivity determined from Pliocene carbon dioxide concentrations. *Nat. Geosci.* **3**, 27–30 (2010).
60. PALEOSENS Project Members, Making sense of palaeoclimate sensitivity. *Nature* **491**, 683–691 (2012).
61. A. M. Haywood *et al.*, Pliocene Model Intercomparison Project (PlioMIP): Experimental design and boundary conditions (experiment 1). *Geosci. Model Dev.* **3**, 227–242 (2010).
62. Z. Zhang, N. E. Zimmermann, J. O. Kaplan, B. Poulter, Modeling spatiotemporal dynamics of global wetlands: Comprehensive evaluation of a new sub-grid TOPMODEL parameterization and uncertainties. *Biogeosciences* **13**, 1387–1408 (2016).
63. N. Gedney, P. Cox, C. Huntingford, Climate feedback from wetland methane emissions. *Geophys. Res. Lett.* **31**, L20503 (2004).
64. P. O. Hopcroft, P. J. Valdes, J. O. Kaplan, Bayesian analysis of the glacial-interglacial methane increase constrained by stable isotopes and Earth system modelling. *Geophys. Res. Lett.* **45**, 3653–3663 (2018).
65. M. G. Sanderson, Biomass of termites and their emission of methane and carbon dioxide: A global database. *Global Biogeochem. Cycles* **10**, 543–557 (1996).
66. A. Arneth, *et al.*, CO_2 inhibition of global terrestrial isoprene emissions: Potential implications for atmospheric chemistry. *Geophys. Res. Lett.* **34**, L18813 (2007).
67. G. Schurgers, A. Arneth, R. Holzinger, A. Goldstein, Process-based modelling of biogenic monoterpene emissions: Sensitivity to temperature and light. *Atmos. Chem. Phys.* **9**, 271–307 (2008).
68. K. Thonicke, S. Venevsky, S. Sitch, W. Cramer, The role of fire disturbance for global vegetation dynamics: Coupling fire into a dynamic global vegetation model. *Global Ecol. Biogeogr.* **10**, 661–677 (2001).
69. R. C. Hudman *et al.*, Steps towards a mechanistic model of global soil nitric oxide emissions: Implementation and space based-constraints. *Atmos. Chem. Phys.* **12**, 7779–7795 (2012).
70. F. Murguia-Flores *et al.*, Soil methanotrophy model (MeMo v1.0): A process-based model to quantify global uptake of atmospheric methane by soil. *Geosci. Model Dev.* **11**, 2009–2032 (2018).